

EGAM: Extended Graph Attention Model for Solving Routing Problems

Licheng Wang¹ Yuzi Yan¹ Mingtao Huang¹ Yuan Shen^{1,2}

Abstract

Neural combinatorial optimization (NCO) solvers, implemented with graph neural networks (GNNs), have introduced new approaches for solving routing problems. Trained with reinforcement learning (RL), the state-of-the-art graph attention model (GAM) achieves near-optimal solutions without requiring expert knowledge or labeled data. In this work, we generalize the existing graph attention mechanism and propose the extended graph attention model (EGAM). Our model utilizes multi-head dot-product attention to update both node and edge embeddings, addressing the limitations of the conventional GAM, which considers only node features. We employ an autoregressive encoder-decoder architecture and train it with policy gradient algorithms that incorporate a specially designed baseline. Experiments show that EGAM matches or outperforms existing methods across various routing problems. Notably, the proposed model demonstrates exceptional performance on highly constrained problems, highlighting its efficiency in handling complex graph structures.

1. Introduction

Routing problems, such as the well-known traveling salesman problem (TSP), represent a fundamental class of combinatorial optimization (CO) problems. Due to the NP-hard nature of routing problems, exact algorithms become computationally prohibitive for large-scale instances (Cappart et al., 2023; Alanzi & Menai, 2025). While hand-crafted heuristics can provide near-optimal solutions for specific problems, they require significant manual effort and lack generalizability (Kim et al., 2021; Bi et al., 2024). Recently, neural combinatorial optimization (NCO) solvers, implemented with graph neural networks (GNNs), have gained

¹Department of Electronic Engineering, Tsinghua University, Beijing, China ²Shanghai Artificial Intelligence Laboratory, Shanghai, China. Correspondence to: Yuan Shen <shenyuan_ee@tsinghua.edu.cn>.

increasing attention due to their ability to autonomously generate effective heuristics (Kool et al., 2019; Wu et al., 2024). Through supervised learning (SL) or reinforcement learning (RL), well-trained NCO solvers strike a strong balance between solution quality and computational efficiency (Kwon et al., 2020; Sun & Yang, 2023).

From a structural perspective, NCO solvers are generally classified into two categories: autoregressive and non-autoregressive (Wu et al., 2024). Autoregressive solvers generate solutions sequentially and are typically trained by RL (Bi et al., 2024). In contrast, non-autoregressive solvers output a heatmap of edge-selection preferences, which requires a subsequent search procedure—such as Monte Carlo Tree Search (Coulom, 2006)—to form the final route (Sun & Yang, 2023). Non-autoregressive solvers are usually trained using SL (Joshi et al., 2022). However, SL is only applicable to problems with labeled data, which is not universally available for all routing scenarios. Given the complex constraints and dynamic nature of real-world route planning, RL-based autoregressive solvers are better suited for practical applications due to their portability in training and deployment (Kwon et al., 2020; Kim et al., 2022).

Among the RL-based NCO solvers, the graph attention model (GAM) (Deudon et al., 2018; Kool et al., 2019) is considered as the state-of-the-art architecture for routing problems. Inspired by Transformer (Vaswani et al., 2017), GAMs utilize multi-head attention (MHA) to aggregate node features over graphs and generate solutions (Kool et al., 2019). Subsequent works, such as POMO (Kwon et al., 2020) and Sym-NCO (Kim et al., 2022), have further enhanced the performance of GAMs by innovating its training algorithm. The Transformer architecture is now widely applied across various machine learning areas, including large language models (LLMs) in natural language processing (NLP) (Naveed et al., 2025) and vision transformers (ViTs) in computer vision (Han et al., 2022). This highlights the effectiveness of the attention mechanisms (particularly multi-head dot-product attention) in extracting representative features from data. However, existing GAMs mainly focus on self-attention between node representations, overlooking the crucial role of edge attributes. This is a significant limitation for problems where edge features are integral, such as the TSP with edge costs. To address this, we design a novel architecture, the extended graph attention

model (EGAM), where both node and edge embeddings are updated via attention mechanism.

From a biological perspective, attention is the process of selectively acquiring information from the environment (Han et al., 2022). Since traditional graph attention methods are limited to operations between nodes (Kim et al., 2022; Bi et al., 2024), why not extend this mechanism to operate between nodes and edges? In our model, we introduce the Node-Edge and Edge-Node Attention operations, where node and edge features are fused through multi-head dot-product attention. Building on these attention mechanisms, we design a model architecture composed of a graph encoder and an autoregressive decoder. The proposed EGAM is capable of performing end-to-end processing, from problem input to route generation. For training, we use the REINFORCE algorithm (Williams, 1992) with a symmetry-based baseline for gradient estimation, enabling parameter training without the need for ground truth.

Compared to traditional GAMs, the EGAM demonstrates advantages in both performance and scalability. We conducted experiments on various routing problems, categorizing them into two types based on the complexity of their constraints. The results show that for problems with simple constraints, EGAM performs similarly to, or slightly better than, state-of-the-art methods. For highly constrained problems, EGAM significantly outperforms state-of-the-art approaches in terms of both solution cost and feasible rate. In the experiments on traveling salesman problem with time window (TSPTW), traveling salesman problem with draft limit (TSPDL), and vehicle routing problem with time window (VRPTW), our model reduced the optimality gap by 2.29%, 2.21%, and 2.04%, respectively, under single-decision settings. These results highlight the efficiency of EGAM in handling complex graph structures. Furthermore, the integration of edge features into the network architecture not only expands the range of solvable problems but also enhances the modeling of complex transition relationships. In summary, we introduce a novel neural network framework for routing problems. The proposed model’s efficiency and scalability provide a promising path toward addressing a broader range of NP-hard CO problems.

2. Related Work

2.1. Neural combinatorial optimization

The application of NCO dates back to Hopfield-networks (Hopfield & Tank, 1985) and deformable template models (Fort, 1988; Angeniol et al., 1988). Recent advancements in neural models and training methods have made NCO a competitive approach for solving CO, particularly in routing problems (I. Garmendia et al., 2024). The Pointer Network (Vinyals et al., 2015) used a recurrent neural network (RNN)

with an attention-based output layer to direct the model’s focus to specific positions in the input sequence. Building on this, Bello et al. (2016) introduced an Actor-Critic algorithm that trained Pointer Networks without labeled data. Additionally, Structure2Vec (Dai et al., 2016; Khalil et al., 2017) employed a neural network to encode graph nodes into high-dimensional embedding vectors, which was trained by Q-learning.

Drawing inspiration from the Transformer architecture (Vaswani et al., 2017), Deudon et al. (2018) first applied GAMs to routing problems, which consisted of a MHA-based encoder to embed graph nodes and an autoregressive decoder to generate solutions. Kool et al. (2019) enhanced this framework by refining the decoder and incorporating a policy gradient algorithm that used a rollout baseline. Subsequent research focused on improving the training algorithms of GAMs. Kwon et al. (2020) introduced POMO, which utilizes multiple decision branches to generate a shared baseline, while Kim et al. (2022) proposed Sym-NCO, a regularizer-based training scheme that leverages inherent symmetry in routing problems. These advancements have further improved the performance of GAMs in solving routing problems, making them state-of-the-art RL-based NCO solvers (Cappart et al., 2023).

In contrast to autoregressive approaches, non-autoregressive architectures do not directly generate solutions but instead produce an adjacency matrix of edge selection preferences (Cappart et al., 2023). Joshi et al. (2019) used graph convolutional networks (GCNs) to output adjacency matrices, with solutions obtained through beam search. Similarly, Kool et al. (2022) introduced a dynamic programming-based decoding strategy, validated on TSP and its variants. Adopting a graph-based diffusion model (Ho et al., 2020), Sun & Yang (2023) proposed DIFUSCO, which achieves near-optimal performance on small-scale TSP instances and maintains its effectiveness on large-scale problems. However, the training of non-autoregressive models relies on labeled data, which is difficult to obtain for complex routing problems.

Additionally, some studies have focused on enhancing the scalability of existing NCO solvers across diverse problem settings and scales. Bi et al. (2024) introduced the Proactive Infeasibility Prevention (PIP) framework, which enhances decision-making by incorporating a learnable preventative infeasibility mask, showing strong performance on constrained problems like TSPTW and TSPDL. To improve generalization for large-scale instances, Fu et al. (2021) proposed a graph sampling-based method to augment pre-trained models. Moreover, Gao et al. (2025) introduced a general selector to allocate problem instances to the most suitable models.

2.2. Attention mechanisms

Attention mechanisms were initially introduced in computer vision as an imitation of the human visual system (Mnih et al., 2014; Guo et al., 2022). In neural machine translation, Bahdanau et al. (2015) proposed an attention-based RNN framework, where the decoder employed an additive attention mechanism to selectively retrieve information from the embedded sequence. Based on this framework, Luong et al. (2015) generalized the mathematical operation of attention mechanisms, introducing the widely used dot-product attention (Niu et al., 2021). Aside from its application in the decoder, attention mechanisms have also been used in RNNs to capture the relationships between input tokens (Cheng et al., 2016; Parikh et al., 2016). Different from previous models, Transformer (Vaswani et al., 2017) presented an architecture eschewing recurrence and instead relying on attention operations for sequence-to-sequence processing. Building on dot-product attention, Vaswani et al. (2017) introduced MHA, which was considered superior to single-head attention for extracting multi-dimensional features. With the input features $\mathbf{X} = [\mathbf{x}_1, \mathbf{x}_2, \dots, \mathbf{x}_M]$, $\mathbf{Y} = [\mathbf{y}_1, \mathbf{y}_2, \dots, \mathbf{y}_N]$, and $\mathbf{Z} = [\mathbf{z}_1, \mathbf{z}_2, \dots, \mathbf{z}_N]$, the MHA is defined by the following formulas:

$$\text{MHA}(\mathbf{X}, \mathbf{Y}, \mathbf{Z}) = \mathbf{W}^O \text{Concat}(\mathbf{H}_1, \mathbf{H}_2, \dots, \mathbf{H}_h), \quad (1)$$

$$\mathbf{H}_i = \text{Attention}(\mathbf{X}^T \mathbf{W}_i^Q, \mathbf{Y}^T \mathbf{W}_i^K, \mathbf{Z}^T \mathbf{W}_i^V)^T. \quad (2)$$

where the attention operation is given by

$$\text{Attention}(\mathbf{Q}, \mathbf{K}, \mathbf{V}) = \text{softmax} \left(\frac{\mathbf{Q}\mathbf{K}^T}{\sqrt{d_k}} \right) \mathbf{V}. \quad (3)$$

In (3), d_k denotes the last dimension of matrix \mathbf{K} . Given that the key and value inputs are often identical, i.e. $\mathbf{Y} = \mathbf{Z}$, we use $\text{MHA}(\mathbf{X}, \mathbf{Y})$ to represent this case.

The Transformer architecture has achieved remarkable success across multiple machine learning domains. Transformer-based models, such as GPT (Radford et al., 2018) and BERT (Devlin et al., 2019), have set new benchmarks in NLP (Naveed et al., 2025). Models like ViT (Dosovitskiy et al., 2021) and DETR (Carion et al., 2020) have demonstrated superior performance in computer vision tasks, including image classification and object detection (Han et al., 2022). The architecture's scalability and ability to capture long-range dependencies have also driven advancements in time-series forecasting, embodied learning, and protein structure prediction (Wang et al., 2024; Khan et al., 2025; Sferrazza et al., 2025).

2.3. Graph attention networks

The concept of graph attention network was first proposed by Veličković et al. (2018) for graph node classification. In their model, named GATs, the additive attention mechanism served as the primary computational tool for processing

graph-structured data (Veličković et al., 2018). Later, Brody et al. (2022) modified the additive attention mechanism and introduced GATv2. GAMs are considered as graph attention networks tailored for routing problems (Kool et al., 2019). Differently, GAMs utilize multi-head dot-product attention to embed graph nodes and generate routing sequences (Deudon et al., 2018; Kool et al., 2019). Other Transformer-based architectures for routing tasks (Kaempfer & Wolf, 2018; Bresson & Laurent, 2021) are also categorized alongside GAMs.

While traditional GATs focus on node representations, Wang et al. (2021) proposed the edge-featured GAT (EGAT), which integrates edge features into the message-passing process by updating edge embeddings using a node-transit strategy. Additionally, Lischka et al. (2024) introduced GREAT, an edge-focused model that incorporates edge information without relying on node embeddings. In contrast, our work extends existing node-based GAMs in a more flexible manner. The proposed EGAM relies on multi-head dot-product attention and defines multiple attention layers for different types of embeddings.

3. Methodology

3.1. Generalized attention mechanism over graphs

We begin by introducing new attention operations for graph-structured data. Conventional GAMs primarily focus on node features. However, edge features also constitute a fundamental aspect of graphs. For example, in the TSP with edge cost, the travelling cost is defined associated with edges, not simply the the distances between nodes. Furthermore, we argue that incorporating edge features can also contribute to solving complex routing problems, such as those with time window constraints. Therefore, we define two novel attention operations: Edge-Node Attention and Node-Edge Attention, which facilitate bidirectional message passing between nodes and edges.

For a full-connected graph $G = (\mathcal{V}, \mathcal{E})$ consisted of N nodes, we assume $\mathcal{V} = \{n_i \mid i = 1, 2, \dots, N\}$ and $\mathcal{E} = \{e_{i,j} \mid i, j = 1, 2, \dots, N\}$. Let \mathbf{n}_i^ℓ and $\mathbf{e}_{i,j}^\ell$ represent the embeddings of node n_i and edge e_{ij} , respectively, as the output of layer ℓ .

Node-Node Attention is the primary operation in existing GAMs for learning node embeddings (Deudon et al., 2018; Kool et al., 2019). The node embeddings are updated as follows:

$$\mathbf{n}_i^\ell = \text{MHA}(\mathbf{n}_i^{\ell-1}, [\mathbf{n}_1^{\ell-1}, \mathbf{n}_2^{\ell-1}, \dots, \mathbf{n}_N^{\ell-1}]). \quad (4)$$

For simplicity, we omit the residual connections (He et al., 2016) and normalization layers (Ioffe & Szegedy, 2015; Ulyanov et al., 2016). MHA operation is permutation-invariant to its input, meaning it is independent of node

ordering, making it well-suited for graph-structured data.

Node-Edge Attention operates between a node and its adjacent edges. Both nodes and edges are embedded into a high-dimensional space \mathbb{R}^{d_m} , enabling the use of the MHA operation as shown in (5). Through Node-Edge Attention, nodes selectively acquire information from their adjacent edges. For undirected graphs, we assume symmetry in the edge embeddings, i.e., $\mathbf{e}_{i,j}^\ell = \mathbf{e}_{j,i}^\ell$. Additionally, self-loops (e.g., $\mathbf{e}_{i,i}^\ell$) are incorporated to allow nodes to attend to their own information, although such edges are explicitly prohibited from being selected during decoding.

$$\mathbf{n}_i^\ell = \text{MHA}(\mathbf{n}_i^{\ell-1}, [\mathbf{e}_{i,1}^{\ell-1}, \mathbf{e}_{i,2}^{\ell-1}, \dots, \mathbf{e}_{i,N}^{\ell-1}]). \quad (5)$$

Edge-Node Attention is the complementary operation to Node-Edge Attention. In undirected graphs, Edge-Node Attention is defined as:

$$\mathbf{e}_{i,j}^\ell = \text{MHA}(\mathbf{e}_{ij}^{\ell-1}, [\mathbf{n}_i^{\ell-1}, \mathbf{n}_j^{\ell-1}]). \quad (6)$$

For directed graphs, additional encoding is required to distinguish between the start and end nodes. Without loss of generality, we use separate linear layers to achieve this distinction:

$$\mathbf{e}_{i,j}^\ell = \text{MHA}(\mathbf{e}_{ij}^{\ell-1}, [\mathbf{W}_s \mathbf{n}_i^{\ell-1} + \mathbf{b}_s, \mathbf{W}_e \mathbf{n}_j^{\ell-1} + \mathbf{b}_e]). \quad (7)$$

Node-Edge Attention and Edge-Node Attention enable bidirectional information propagation between nodes and edges through MHA. In contrast to the linear and activation operations in GCNs (Joshi et al., 2022), we argue that MHA more efficiently performs the fusion and interaction of multi-dimensional features. The proposed graph attention mechanism facilitates a more effective representation of graph structures while also being used during the decoding phase to capture dynamic context information. Additionally, this attention mechanism can be easily adapted to non-fully-connected graphs by incorporating masks into the MHA.

3.2. Extended graph attention model

Based on the aforementioned attention mechanism, we design a new autoregressive architecture for routing problems. The proposed EGAM adopts an encoder-decoder framework, where the encoder embeds the input graph, and the decoder sequentially outputs the node sequence.

For a routing problem instance, denoted as \mathbf{s} , we represent its topological structure using a graph $G = (\mathcal{V}, \mathcal{E})$. The initial node features and edge features are respectively denoted as $\mathbf{n}_i^{\text{init}} \in \mathbb{R}^{F_n}$ and $\mathbf{e}_{i,j}^{\text{init}} \in \mathbb{R}^{F_e}$, respectively. The goal is to find a route (solution) $\boldsymbol{\pi}$ that minimizes the cost $C(\boldsymbol{\pi}, \mathbf{s})$, where $\boldsymbol{\pi} = [\pi_1, \pi_2, \dots, \pi_T], \pi_t \in \mathcal{V}, t = 1, 2, \dots, T$. In autoregressive NCO solvers (Kool et al., 2019; Bi et al., 2024), the output of the neural network is modeled as a conditional probability distribution $p_\theta(\pi_t | \boldsymbol{\pi}_{<t}, \mathbf{s})$, where θ denotes the network parameters.

The structure of EGAM is illustrated in Figure 1. The role of the encoder in EGAM is to map the graph elements into a high-dimensional space, providing embeddings for the decoder’s decision-making process. The input features are first transformed by a linear embedding layer:

$$\mathbf{n}_i^0 = \mathbf{W}_n^{\text{init}} \mathbf{n}_i^{\text{init}} + \mathbf{b}_n^{\text{init}}, \quad (8)$$

$$\mathbf{e}_{i,j}^0 = \mathbf{W}_e^{\text{init}} \mathbf{e}_{i,j}^{\text{init}} + \mathbf{b}_e^{\text{init}}, \quad (9)$$

where $\mathbf{W}_n^{\text{init}} \in \mathbb{R}^{d_m \times F_n}, \mathbf{W}_e^{\text{init}} \in \mathbb{R}^{d_m \times F_e}, \mathbf{b}_n^{\text{init}}, \mathbf{b}_e^{\text{init}} \in \mathbb{R}^{d_m}$. We set the embedding dimension $d_m = 128$. After the initial layer, the node and edge embeddings are updated using the graph attention mechanism formalized in Equations (4) to (7). Our model employs integrated attention layers that sequentially processes Node-Node, Edge-Node, and Node-Edge attention operations. We retain the existing Node-Node attention to ensure efficient information propagation across nodes. The newly introduced Edge-Node and Node-Edge attention mechanisms incorporate edge embeddings into the graph representation learning process. We consider edge embeddings crucial for capturing important transition relationships in routing problems, particularly those involving energy or time constraints. Specifically, the MHA mechanism uses $h = 8$ heads, with the last dimension of $\mathbf{Q}, \mathbf{K}, \mathbf{V}$ being $d_q = d_k = d_v = 16$. After the attention layers, we apply a node-wise feed-forward (FF) layer (Vaswani et al., 2017). The FF layer is composed of two linear layers and a ReLU activation with dimension $d_{\text{ff}} = 512$. Residual connections (He et al., 2016) and instance normalization (Ulyanov et al., 2016) are applied to both the integrated attention layer and the FF layer. Finally, the graph embeddings $\{\mathbf{n}_i^L\}_{i=1,2,\dots,N}$ and $\{\mathbf{e}_{i,j}^L\}_{i,j=1,2,\dots,N}$ are generated after L encoder layers.

The decoder leverages the graph embeddings and context to generate the probability distribution for the next node. The context embedding layer is responsible for encoding the context information at the current time step t . The composition of context depends on the specific problem setting. For example, in the TSP, the context includes the embeddings of the current node and the starting node:

$$\hat{\mathbf{n}}_c = \text{Concat}(\mathbf{n}_{\pi_{t-1}}^L, \mathbf{n}_{\pi_1}^L). \quad (10)$$

In the case of the capacitated vehicle routing problem (CVRP), where the starting node is fixed, the context includes the current node embedding along with the remaining vehicle capacity:

$$\hat{\mathbf{n}}_c = \text{Concat}(\mathbf{n}_{\pi_{t-1}}^L, \text{Cap}(\boldsymbol{\pi}_{<t}, \mathbf{s})). \quad (11)$$

We provide further context details on different routing problems in Appendix B. A linear Layer is used to project the context vector into the embedding space:

$$\mathbf{n}_c^0 = \mathbf{W}_c \hat{\mathbf{n}}_c + \mathbf{b}_c. \quad (12)$$

The attention mechanism is also incorporated in our de-

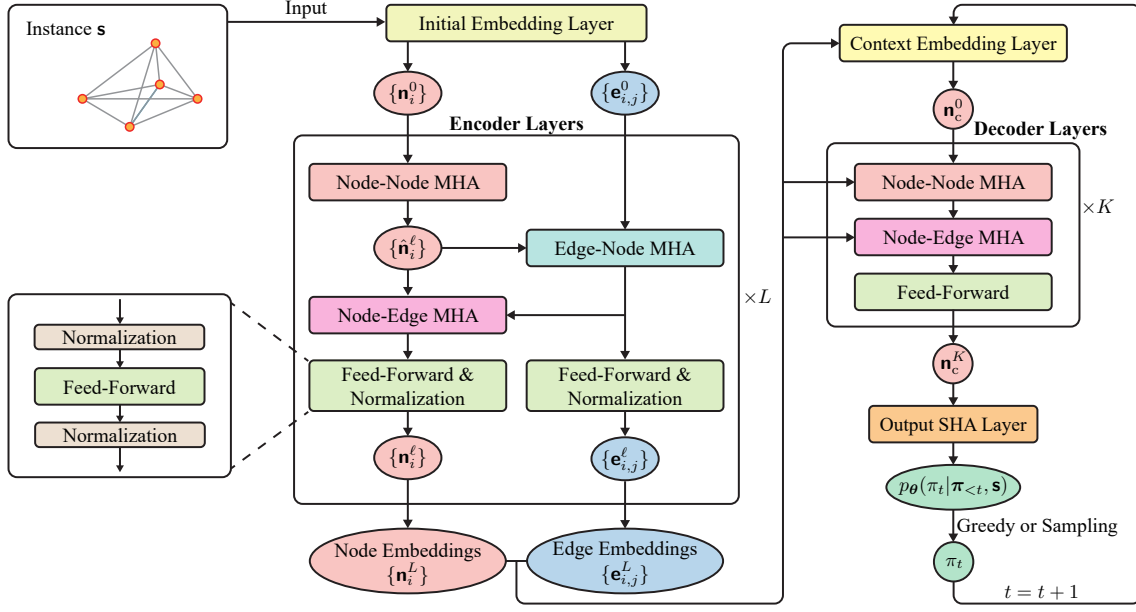


Figure 1. Illustration of the proposed EGAM structure. The rounded rectangles represent trainable network layers, while the ellipses denote the output variables. For simplicity, the residual connections of the MHA and feed-forward layers are omitted. Arrows indicate the data flow from the problem input to the sequence generation. In a single decision process, the encoder runs only once, while the decoder operates repeatedly until the full route is generated.

coder for decision-making. First, the context embedding is updated through integrated attention layers, which consist of Node-Node and Node-Edge attention. These layers enable \mathbf{n}_c^0 to gather information from adjacent nodes $\{\mathbf{n}_i^L\}_{i=1,2,\dots,N}$ and edges $\{\mathbf{e}_{\pi_{t-1},j}^L\}_{j=1,2,\dots,N}$. To ensure that only feasible nodes are considered, we apply masks to the attention operations. The final probability is computed via a single-head attention layer. We perform a dot-product attention operation between the context embedding and adjacent edge embeddings. The query and keys are projected using parameter matrices $\mathbf{W}_{\text{out}}^q, \mathbf{W}_{\text{out}}^k \in \mathbb{R}^{d_m \times d_m}$:

$$\mathbf{q}_c = \mathbf{W}_{\text{out}}^q \mathbf{n}_c^K, \quad \mathbf{k}_j = \mathbf{W}_{\text{out}}^k \mathbf{e}_{\pi_{t-1},j}^L. \quad (13)$$

We then apply a clipped tanh function to restrict the range of the attention weights, followed by a softmax function to compute the final probabilities:

$$u_j = \begin{cases} \alpha \cdot \tanh\left(\frac{\mathbf{q}_c^T \mathbf{k}_j}{\sqrt{d_m}}\right), & \text{if node } j \text{ is feasible} \\ -\infty, & \text{otherwise} \end{cases} \quad (14)$$

$$p_{\theta}(\pi_t = n_i | \pi_{<t}, \mathbf{s}) = \text{softmax}_i(u_1, u_2, \dots, u_N). \quad (15)$$

The node sequence is decoded from $p_{\theta}(\pi_t | \pi_{<t}, \mathbf{s})$ using two strategies: sampling and greedy. During training, we adopt the sampling strategy to encourage exploration within the feasible region. During validation and testing, the greedy strategy selects the node with the highest probability at each step to generate a single trajectory. In contrast, the sampling

strategy randomly selects nodes based on probabilities, producing multiple results at the cost of increased computation time.

3.3. Reinforcement learning with symmetry-based baseline

We train the proposed model using the REINFORCE algorithm (Williams, 1992) with a symmetry-based baseline. REINFORCE is a classic policy gradient algorithm that estimates the gradient by evaluating the cost of an entire trajectory. The loss function is defined as $\mathcal{L}(\theta | \mathbf{s}) = \mathbb{E}_{p_{\theta}(\pi | \mathbf{s})} [C(\pi, \mathbf{s})]$, where p_{θ} represents the probability of generating a solution π for a given instance \mathbf{s} :

$$p_{\theta}(\pi | \mathbf{s}) = p(\pi_1) \prod_{t=2}^T p_{\theta}(\pi_t | \pi_{<t}, \mathbf{s}). \quad (16)$$

The REINFORCE gradient estimator is then expressed as:

$$\nabla \mathcal{L}(\theta | \mathbf{s}) = \mathbb{E}_{p_{\theta}(\pi | \mathbf{s})} [(C(\pi, \mathbf{s}) - b(\mathbf{s})) \nabla \log p_{\theta}(\pi | \mathbf{s})] \quad (17)$$

The baseline function $b(\mathbf{s})$ is introduced to provide a reference cost for each instance. A well-designed baseline can significantly improve training efficiency and accelerate convergence. (Sutton & Barto, 1998; Kim et al., 2022).

We adopt a baseline function derived from the symmetries in routing problems (Kim et al., 2022), including starting

point symmetry, sampling symmetry, and graph symmetry. Starting point symmetry applies to problems like the TSP, where no fixed starting point is specified, suggesting that the optimal solution should remain invariant regardless of the selected starting node (Kwon et al., 2020). Sampling symmetry asserts that the expected cost should remain consistent across multiple trajectories sampled from the model’s output for a given instance. Finally, graph symmetry concerns the relative topological relationships within the graph structure, implying that the model should produce similar solution sequences for instances that are equivalent under transformations like rotation or reflection, as the underlying problem remains unchanged (Kim et al., 2022).

Computationally, we combine starting point and sampling symmetry. For TSP, the starting point is sampled from a uniform distribution, i.e., $p(\pi_1 = n_i) = 1/N$. For a given instance \mathbf{s} , we generate m equivalent problems by applying random rotations and reflections. The model then produces n solutions for each transformed instance under its sampling policy. The baseline $b(\mathbf{s})$ is estimated as the mean cost across the $m \times n$ solutions:

$$b(\mathbf{s}) \approx \frac{1}{mn} \sum_{i=1}^m \sum_{j=1}^n C(\pi^{i,j}, \mathbf{s}^i), \quad (18)$$

where $\{\mathbf{s}^i\}$ are equivalent problems of \mathbf{s} , and $\{\pi^{i,j}\}$ are the solutions sampled for \mathbf{s}^i . Therefore, the gradient of $\mathcal{L}(\theta|\mathbf{s})$ is estimated by:

$$\nabla \mathcal{L}(\theta|\mathbf{s}) \approx \frac{1}{mn} \sum_{i=1}^m \sum_{j=1}^n [(C(\pi^{i,j}, \mathbf{s}^i) - b(\mathbf{s})) \nabla \log p_\theta]. \quad (19)$$

By leveraging the symmetries described above, our baseline function effectively augments the input instances, enhancing sample utilization. The designed $b(\mathbf{s})$ establishes a relative benchmark for evaluating the cost of the model’s outputs. Experimental results demonstrate that this baseline construction method achieves better convergence performance compared to the deterministic greedy rollout approach (Kool et al., 2019; Kim et al., 2022). Based on the gradient expression in Equation (19), we employ the Adam optimizer (Kingma & Ba, 2015) to learn the model parameters.

3.4. Scalability

In the previous sections, we established the autoregressive structure of EGAM and the reinforcement learning training framework. Notably, our model also retains the ability to be extended into a non-autoregressive mode. By preserving the Encoder for embedding the graph structure, a modified decoder can be employed to output routing planning heatmaps. Furthermore, the modified model can be trained using SL (Sun & Yang, 2023; Luo et al., 2023). The proposed framework is also adaptable to additional methods

aimed at assisting decision-making in graph neural networks (Fu et al., 2021; Bi et al., 2024; Xia et al., 2024), thereby enhancing generalization across diverse problem settings and scales.

4. Experiments

We evaluated the proposed model on several routing problems, setting the number of nodes to 50. Based on the complexity of the constraints, the experiments were divided into two groups: (1) TSP, CVRP, and prize collecting traveling salesman problem (PCTSP), which feature relatively simple constraints and minimal restrictions on the node sequence; and (2) TSPTW, TSPDL, and VRPTW, which involve more challenging constraints, such as time windows and draft limits, making solution feasibility highly sensitive to the ordering of nodes. During the model training phase, the experiments were conducted on four NVIDIA RTX 3090 (24GB) GPUs. Our model uses four encoder layers and one decoder layer. The batch size was set to 128, with each epoch containing 2500 batches. The model was trained for 100 epochs, with the learning rate $\eta = 10^{-4}$ for the first 90 epochs and $\eta = 10^{-5}$ for the last 10 epochs. For the testing phase, a single GPU was used to ensure a fair comparison of time complexity with traditional search-based methods.

We considered two categories of comparative algorithms: (1) Traditional routing problem solvers, including LKH-3¹ (Helsgaun, 2017), Gurobi² (Gurobi Optimization), and OR-Tools³ (Google). The performance of these solvers was validated on a CPU with 64 cores. LKH-3 is a well-established heuristic solver, often regarded as capable of obtaining almost optimal solutions for problems where it is applicable. Gurobi employs the branch-and-bound method to find exact solutions to combinatorial optimization problems. OR-Tools is another widely used solver, where the quality of the results depends on the search time. We evaluated OR-Tools’ performance under different time limits to provide a comprehensive reference. (2) Learning-based methods, including GAM (Kool et al., 2019; Bi et al., 2024), GATv2 (Brody et al., 2022), POMO (Kwon et al., 2020; Bi et al., 2024), and Sym-NCO (Kim et al., 2022). We evaluated both greedy and sampling inference strategies during the testing phase. The greedy strategy generates a single trajectory, directly reflecting the performance of NCO solvers. The sampling strategy involves input augmentation and repeated experiments to select the best trajectory. For different methods, we employed two sampling modes: repeating the sampling process 1280 times, or using input augmentation 8 times followed by 20 repetitions of the decision process.

¹<http://webhotel4.ruc.dk/~keld/research/LKH-3/>

²<https://www.gurobi.com/solutions/gurobi-optimizer/>

³<https://developers.google.com/optimization/routing/>

Table 1. Experimental results on TSP, CVRP and PCTSP. The downward arrows in the metrics indicate that smaller values are better. A '/' denotes that the method is not applicable or has not been applied to the corresponding problem. The optimal methods under the greedy and sampling strategies for learning-based approaches are highlighted in bold.

Method	Type	TSP			CVRP			PCTSP		
		Cost↓	Gap↓	Time↓	Cost↓	Gap↓	Time↓	Cost↓	Gap↓	Time↓
LKH-3	Heuristic	5.70	0.00%	1.3m	10.38	0.00%	57m	/	/	/
Gurobi	Branch and Bound	5.70	0.00%	30m	/	/	/	4.47	0.00%	58m
OR-Tools (1m)	Heuristic	5.70	0.00%	2.6h	10.56	1.78%	2.6h	4.48	0.07%	2.6h
OR-Tools (10m)	Heuristic	5.70	0.00%	1.1d	10.42	0.42%	1.1d	4.47	0.00%	1.1d
GAM	Greedy	5.80	1.76%	4s	10.98	5.86%	4s	4.60	2.84%	3s
GATv2	Greedy	5.77	1.33%	3s	10.90	5.04%	3s	4.56	1.95%	2s
POMO	Greedy	5.73	0.64%	5s	10.74	3.54%	6s	/	/	/
Sym-NCO	Greedy	5.73	0.57%	4s	10.73	3.42%	4s	4.52	1.07%	4s
EGAM (Ours)	Greedy	5.72	0.49%	6s	10.72	3.29%	7s	4.51	0.81%	6s
GAM	1280 Sampling	5.73	0.52%	5.4m	10.62	2.40%	6.1m	4.52	1.05%	4.2m
GATv2	1280 Sampling	5.72	0.33%	3.2m	10.59	2.05%	3.8m	4.50	0.55%	2.5m
POMO	8×20 Sampling	5.70	0.06%	2.7m	10.47	0.98%	2.9m	/	/	/
Sym-NCO	8×20 Sampling	5.70	0.04%	1.4m	10.47	0.94%	1.6m	4.48	0.25%	1.3m
EGAM (Ours)	8×20 Sampling	5.70	0.03%	2.2m	10.48	1.01%	2.4m	4.48	0.11%	2.3m

Table 2. Experimental results on TSPTW and TSPDL. Notations are the same with Table 1.

Method	Type	TSPTW				TSPDL			
		Cost↓	Infeasible↓	Gap↓	Time↓	Cost↓	Infeasible↓	Gap↓	Time↓
LKH-3	Heuristic	13.01	0.00%	0.00%	1.1h	10.86	0.00%	0.00%	1.4h
OR-Tools (10m)	Heuristic	13.05	15.52%	0.30%	22h	/	/	/	/
GAM	Greedy	14.58	20.86%	12.06%	4s	12.43	10.27%	14.41%	4s
GATv2	Greedy	14.48	18.60%	11.32%	3s	11.97	10.43%	10.25%	3s
POMO	Greedy	14.07	14.92%	8.13%	5s	11.69	7.60%	7.67%	5s
Sym-NCO	Greedy	14.10	17.88%	8.39%	4s	11.70	3.74%	7.71%	4s
EGAM (Ours)	Greedy	13.77	7.76%	5.84%	6s	11.45	1.14%	5.46%	5s
GAM	1280 Sampling	13.90	0.74%	6.83%	5.5m	11.82	1.21%	8.86%	5.6m
GATv2	1280 Sampling	13.66	0.33%	4.97%	3.2m	11.38	0.10%	4.75%	3.1m
POMO	8×20 Sampling	13.54	0.68%	4.06%	2.8m	11.32	1.46%	4.26%	3.0m
Sym-NCO	8×20 Sampling	13.49	0.37%	3.69%	1.5m	11.30	0.51%	4.03%	1.5m
EGAM (Ours)	8×20 Sampling	13.42	0.31%	3.19%	2.2m	11.19	0.09%	3.02%	2.2m

4.1. TSP & CVRP & PCTSP

We selected TSP, CVRP and PCTSP as representatives of routing problems with relatively simple constraints. The TSP aims to find the shortest route that visits each location exactly once and returns to the origin. The CVRP extends the TSP by introducing vehicle capacity constraints, requiring routes to serve customer nodes without exceeding vehicle capacity. Vehicles must return to the depot to unload when their capacity is reached, with the objective of minimizing the total travel distance. The PCTSP builds upon the TSP by associating each node with a prize and a penalty, aiming to collect prizes from visited nodes while minimizing penalties for skipped nodes. A feasible tour ensures the total prize meets a predetermined threshold, with the overall cost being the sum of the tour length and penalties for omitted nodes. Further details on these problems are

provided in the Appendix B. Our testing set includes 10,000 randomly generated instances for each problem, and the large-scale dataset helps mitigate performance variations caused by randomness.

The experimental results on the TSP, CVRP, and PCTSP are presented in Table 1. We report the average cost, average optimality gap, and total computation time for each method across each problem’s testing set. As can be observed, our model consistently outperforms other NCO solvers under the greedy strategy. Notably, EGAM shows a slight advantage over the state-of-the-art approaches POMO and Sym-NCO. Under the sampling strategy, EGAM, POMO, and Sym-NCO perform almost identically, while EGAM maintains a clear advantage over GAM and GATv2. In the case of CVRP under the sampling strategy, EGAM performs slightly worse than Sym-NCO, but the difference is only

Table 3. Experimental results on VRPTW. Notations are the same with Table 1 and Table 2.

Method	VRPTW		
	Cost↓	Gap↓	Time↓
OR-Tools (1m)	20.03	8.91%	2.6h
OR-Tools (10m)	19.07	3.70%	1.1d
OR-Tools (60m)	18.39	0.00%	6.4d
GAM (Greedy)	21.46	16.71%	3s
GATv2 (Greedy)	20.48	11.36%	2s
Sym-NCO (Greedy)	19.97	8.62%	3s
EGAM (Ours, Greedy)	19.60	6.58%	5s
GAM (1280 Sampling)	19.47	5.90%	3.9m
GATv2 (1280 Sampling)	19.12	3.97%	2.5m
Sym-NCO (8×20 Sampling)	18.96	3.12%	1.2m
EGAM (Ours, 8×20 Sampling)	18.83	2.45%	1.9m

0.07%, which we attribute to the training process focusing on optimizing single-decision performance. In summary, for these three problems with simple constraints, EGAM either matches or slightly outperforms state-of-the-art methods.

4.2. TSPTW & TSPDL & VRPTW

TSPTW introduces time window constraints on the nodes to be visited. Each node must be visited within its designated time window; otherwise, the visit is considered a failure. If arrival occurs earlier than the start of the time window, the agent must wait until the window opens. A tour is feasible only if all nodes are visited while adhering to these time constraints. During data generation, we ensure that feasible solutions exist. For learning-based methods, we incorporate a penalty term for time window violations, guiding the model to focus on learning feasible solutions. TSPDL involves ship routing, where each port (node) has a cargo capacity demand and a draft limit. The goal is to plan a route such that the ship’s load at each port does not exceed its draft limit. Similarly, we introduce penalties for violations of the draft limit. For VRPTW, we relax the constraint of visiting all nodes. The objective is modified to visit as many nodes as possible within their time windows. During data generation, we allow time window conflicts, which aligns more closely with real-world scenarios. The cost function is set to the number of nodes that were not successfully visited. In addition to the previously mentioned metrics, we also report the infeasibility rates for TSPTW and TSPDL. Each problem’s testing set consists of 10,000 instances.

The experimental results on TSPTW and TSPDL are presented in Table 2. The results demonstrate that EGAM significantly outperforms other NCO methods in both cost and infeasible rate. Specifically, under a single-decision (greedy) setting, EGAM reduces the optimality gap by 2.29% and the infeasible rate by 7.16% compared to POMO on TSPTW. For TSPDL, EGAM also achieves reductions of 2.21% in

optimality gap and 2.60% in infeasible rate compared to the strongest baselines. When employing the sampling strategy, EGAM remains superior to all comparative algorithms. Notably, while achieving lower costs, it reduces the infeasible rates on TSPTW and TSPDL to 0.31% and 0.09%, respectively. The experimental results on VRPTW are presented in Table 3. Since the problem formulation we consider falls outside the solvable scope of LKH-3, we use OR-Tools with a search time limit of one hour to provide an approximate reference for optimal values. Compared to Sym-NCO, EGAM reduces the cost by 2.04% under the greedy strategy and by 0.67% under the sampling strategy. Furthermore, the sampling results from EGAM surpass those obtained by OR-Tools with a 10-minute limit, while being approximately 800 times faster.

In Appendix C, we provide additional experiments and analyses, including training dynamics, the impact of model size, and generalization tests. We intend to release our source code publicly to support reproducibility and foster collaboration within the research community in the future.

5. Conclusion

In this paper, we proposed a novel neural network framework, EGAM, designed for routing problems. We introduced generalized graph attention mechanism and applied it to graph embedding and autoregressive decision-making. The model was trained using RL with a symmetry-based baseline, requiring no expert knowledge or labeled data. Experimental results demonstrated that EGAM matched or surpassed existing RL-based NCO solvers across a variety of routing problems. Notably, EGAM exhibits particularly strong performance on highly constrained problems such as TSPTW, TSPDL, and VRPTW. Our future work will focus on the scalability of EGAM, including the following directions: (1) integrating improved methods tailored for NCO to enhance performance on specific problem types and larger-scale instances; (2) extending its application to a wider variety of routing problems, such as edge-based route planning; (3) exploring additional training paradigms, such as SL; and (4) generalizing the approach beyond routing problems to tackle a wider variety of combinatorial optimization tasks, with the goal of establishing a universal framework for graph-structured problems.

Impact Statement

This paper presents work whose goal is to advance the field of Machine Learning. There are many potential societal consequences of our work, none of which we feel must be specifically highlighted here.

References

Alanzi, E. and Menai, M. E. B. Solving the traveling salesman problem with machine learning: a review of recent advances and challenges. *Artificial Intelligence Review*, 58(9):267, 2025.

Angeniol, B., Vaubois, G. D. L. C., and Le Texier, J.-Y. Self-organizing feature maps and the travelling salesman problem. *Neural Networks*, 1(4):289–293, 1988.

Bahdanau, D., Cho, K., and Bengio, Y. Neural machine translation by jointly learning to align and translate. In *International Conference on Learning Representations*, 2015.

Bello, I., Pham, H., Le, Q. V., Norouzi, M., and Bengio, S. Neural combinatorial optimization with reinforcement learning. *arXiv preprint arXiv:1611.09940*, 2016.

Bi, J., Ma, Y., Zhou, J., Song, W., Cao, Z., Wu, Y., and Zhang, J. Learning to handle complex constraints for vehicle routing problems. *Advances in Neural Information Processing Systems*, 37:93479–93509, 2024.

Bresson, X. and Laurent, T. The transformer network for the traveling salesman problem. *arXiv preprint arXiv:2103.03012*, 2021.

Brody, S., Alon, U., and Yahav, E. How attentive are graph attention networks? In *International Conference on Learning Representations*, 2022.

Cappart, Q., Chételat, D., Khalil, E. B., Lodi, A., Morris, C., and Veličković, P. Combinatorial optimization and reasoning with graph neural networks. *Journal of Machine Learning Research*, 24(130):1–61, 2023.

Carion, N., Massa, F., Synnaeve, G., Usunier, N., Kirillov, A., and Zagoruyko, S. End-to-end object detection with transformers. In *European conference on computer vision*, pp. 213–229. Springer, 2020.

Cheng, J., Dong, L., and Lapata, M. Long short-term memory-networks for machine reading. In *Proceedings of the 2016 Conference on Empirical Methods in Natural Language Processing*. Association for Computational Linguistics, 2016.

Coulom, R. Efficient selectivity and backup operators in monte-carlo tree search. In *International conference on computers and games*, pp. 72–83. Springer, 2006.

Dai, H., Dai, B., and Song, L. Discriminative embeddings of latent variable models for structured data. In *International Conference on Machine Learning*, pp. 2702–2711. PMLR, 2016.

Deudon, M., Cournut, P., Lacoste, A., Adulyasak, Y., and Rousseau, L.-M. Learning heuristics for the tsp by policy gradient. In *International Conference on Integration of Constraint Programming, Artificial Intelligence, and Operations Research*, pp. 170–181. Springer, 2018.

Devlin, J., Chang, M.-W., Lee, K., and Toutanova, K. Bert: Pre-training of deep bidirectional transformers for language understanding. In *Proceedings of the 2019 Conference of the North American Chapter of the Association for Computational Linguistics: Human Language Technologies, Volume 1 (Long and Short papers)*, pp. 4171–4186, 2019.

Dosovitskiy, A., Beyer, L., Kolesnikov, A., Weissenborn, D., Zhai, X., Unterthiner, T., Dehghani, M., Minderer, M., Heigold, G., Gelly, S., Uszkoreit, J., and Houlsby, N. An image is worth 16x16 words: Transformers for image recognition at scale. In *International Conference on Learning Representations*, 2021.

Fort, J. Solving a combinatorial problem via self-organizing process: An application of the kohonen algorithm to the traveling salesman problem. *Biological cybernetics*, 59(1):33–40, 1988.

Fu, Z.-H., Qiu, K.-B., and Zha, H. Generalize a small pre-trained model to arbitrarily large tsp instances. In *Proceedings of the AAAI Conference on Artificial Intelligence*, volume 35, pp. 7474–7482, 2021.

Gao, C., Shang, H., Xue, K., and Qian, C. Neural solver selection for combinatorial optimization. In *International Conference on Machine Learning*, 2025.

Guo, M.-H., Xu, T.-X., Liu, J.-J., Liu, Z.-N., Jiang, P.-T., Mu, T.-J., Zhang, S.-H., Martin, R. R., Cheng, M.-M., and Hu, S.-M. Attention mechanisms in computer vision: A survey. *Computational visual media*, 8(3):331–368, 2022.

Han, K., Wang, Y., Chen, H., Chen, X., Guo, J., Liu, Z., Tang, Y., Xiao, A., Xu, C., Xu, Y., et al. A survey on vision transformer. *IEEE Transactions on Pattern Analysis and Machine Intelligence*, 45(1):87–110, 2022.

He, K., Zhang, X., Ren, S., and Sun, J. Deep residual learning for image recognition. In *Proceedings of the IEEE Conference on Computer Vision and Pattern Recognition*, pp. 770–778, 2016.

Helsgaun, K. An extension of the Lin-Kernighan-Helsgaun TSP solver for constrained traveling salesman and vehicle routing problems. Technical report, Roskilde University, 2017.

Ho, J., Jain, A., and Abbeel, P. Denoising diffusion probabilistic models. *Advances in Neural Information Processing Systems*, 33:6840–6851, 2020.

Hopfield, J. J. and Tank, D. W. “neural” computation of decisions in optimization problems. *Biological cybernetics*, 52(3):141–152, 1985.

I. Garmendia, A., Ceberio, J., and Mendiburu, A. Applicability of neural combinatorial optimization: a critical view. *ACM Transactions on Evolutionary Learning and Optimization*, 4(3):1–26, 2024.

Ioffe, S. and Szegedy, C. Batch normalization: Accelerating deep network training by reducing internal covariate shift. In *International Conference on Machine Learning*, pp. 448–456. PMLR, 2015.

Joshi, C. K., Laurent, T., and Bresson, X. An efficient graph convolutional network technique for the travelling salesman problem. *arXiv preprint arXiv:1906.01227*, 2019.

Joshi, C. K., Cappart, Q., Rousseau, L.-M., and Laurent, T. Learning the travelling salesperson problem requires rethinking generalization. *Constraints*, 27:70–98, 2022.

Kaempfer, Y. and Wolf, L. Learning the multiple traveling salesmen problem with permutation invariant pooling networks. *arXiv preprint arXiv:1803.09621*, 2018.

Khalil, E., Dai, H., Zhang, Y., Dilksina, B., and Song, L. Learning combinatorial optimization algorithms over graphs. *Advances in Neural Information Processing Systems*, 30, 2017.

Khan, S., Noor, S., Awan, H. H., Iqbal, S., AlQahtani, S. A., Dilshad, N., and Ahmad, N. Deep-probind: binding protein prediction with transformer-based deep learning model. *BMC Bioinformatics*, 26(1):88, 2025.

Kim, M., Park, J., et al. Learning collaborative policies to solve np-hard routing problems. *Advances in Neural Information Processing Systems*, 34:10418–10430, 2021.

Kim, M., Park, J., and Park, J. Sym-nco: Leveraging symmetry for neural combinatorial optimization. *Advances in Neural Information Processing Systems*, 35: 1936–1949, 2022.

Kingma, D. P. and Ba, J. L. Adam: A method for stochastic optimization. In *International Conference on Learning Representations*, 2015.

Kool, W., van Hoof, H., and Welling, M. Attention, learn to solve routing problems! In *International Conference on Learning Representations*, 2019.

Kool, W., van Hoof, H., Gromicho, J., and Welling, M. Deep policy dynamic programming for vehicle routing problems. In *International Conference on Integration of Constraint Programming, Artificial Intelligence, and Operations Research*, pp. 190–213. Springer, 2022.

Kwon, Y.-D., Choo, J., Kim, B., Yoon, I., Gwon, Y., and Min, S. Pomo: Policy optimization with multiple optima for reinforcement learning. *Advances in Neural Information Processing Systems*, 33:21188–21198, 2020.

Lischka, A., Rydin, F., Wu, J., Chehreghani, M. H., and Kulcsár, B. A great architecture for edge-based graph problems like tsp. *arXiv preprint arXiv:2408.16717*, 2024.

Luo, F., Lin, X., Liu, F., Zhang, Q., and Wang, Z. Neural combinatorial optimization with heavy decoder: Toward large scale generalization. *Advances in Neural Information Processing Systems*, 36:8845–8864, 2023.

Luo, F., Lin, X., Wang, Z., Tong, X., Yuan, M., and Zhang, Q. Self-improved learning for scalable neural combinatorial optimization. *arXiv preprint arXiv:2403.19561*, 2024.

Luong, T., Pham, H., and Manning, C. D. Effective approaches to attention-based neural machine translation. In *Proceedings of the 2015 Conference on Empirical Methods in Natural Language Processing*, pp. 1412. Association for Computational Linguistics, 2015.

Mnih, V., Heess, N., Graves, A., and Kavukcuoglu, K. Recurrent models of visual attention. *Advances in Neural Information Processing Systems*, 27, 2014.

Naveed, H., Khan, A. U., Qiu, S., Saqib, M., Anwar, S., Usman, M., Akhtar, N., Barnes, N., and Mian, A. A comprehensive overview of large language models. *ACM Transactions on Intelligent Systems and Technology*, 16 (5):1–72, 2025.

Niu, Z., Zhong, G., and Yu, H. A review on the attention mechanism of deep learning. *Neurocomputing*, 452:48–62, 2021.

Parikh, A., Täckström, O., Das, D., and Uszkoreit, J. A decomposable attention model for natural language inference. In *Proceedings of the 2016 Conference on Empirical Methods in Natural Language Processing*, pp. 2249–2255, 2016.

Radford, A., Narasimhan, K., Salimans, T., and Sutskever, I. Improving language understanding by generative pre-training. *OpenAI Blog*, 2018.

Sferrazza, C., Huang, D.-M., Liu, F., Lee, J., and Abbeel, P. Body transformer: Leveraging robot embodiment for policy learning. In *Conference on Robot Learning*, pp. 3407–3424. PMLR, 2025.

Sun, Z. and Yang, Y. Difusco: Graph-based diffusion solvers for combinatorial optimization. *Advances in Neural Information Processing Systems*, 36:3706–3731, 2023.

Sutton, R. S. and Barto, A. G. *Reinforcement learning: An introduction*, volume 1. MIT press Cambridge, 1998.

Ulyanov, D., Vedaldi, A., and Lempitsky, V. Instance normalization: The missing ingredient for fast stylization. *arXiv preprint arXiv:1607.08022*, 2016.

Vaswani, A., Shazeer, N., Parmar, N., Uszkoreit, J., Jones, L., Gomez, A. N., Kaiser, Ł., and Polosukhin, I. Attention is all you need. *Advances in Neural Information Processing Systems*, 30, 2017.

Veličković, P., Cucurull, G., Casanova, A., Romero, A., Liò, P., and Bengio, Y. Graph attention networks. In *International Conference on Learning Representations*, 2018.

Vinyals, O., Fortunato, M., and Jaitly, N. Pointer networks. *Advances in Neural Information Processing Systems*, 28, 2015.

Wang, Y., Wu, H., Dong, J., Qin, G., Zhang, H., Liu, Y., Qiu, Y., Wang, J., and Long, M. Timexer: Empowering transformers for time series forecasting with exogenous variables. *Advances in Neural Information Processing Systems*, 37:469–498, 2024.

Wang, Z., Chen, J., and Chen, H. Egat: Edge-featured graph attention network. In *International Conference on Artificial Neural Networks*, pp. 253–264. Springer, 2021.

Williams, R. J. Simple statistical gradient-following algorithms for connectionist reinforcement learning. *Machine learning*, 8(3):229–256, 1992.

Wu, X., Wang, D., Wen, L., Xiao, Y., Wu, C., Wu, Y., Yu, C., Maskell, D. L., and Zhou, Y. Neural combinatorial optimization algorithms for solving vehicle routing problems: A comprehensive survey with perspectives. *arXiv preprint arXiv:2406.00415*, 2024.

Xia, Y., Yang, X., Liu, Z., Liu, Z., Song, L., and Bian, J. Position: Rethinking post-hoc search-based neural approaches for solving large-scale traveling salesman problems. In *International Conference on Machine Learning*, pp. 54178–54190. PMLR, 2024.

Xiao, P., Zhang, Z., Chen, J., Wang, J., and Zhang, Z. Neural combinatorial optimization for robust routing problem with uncertain travel times. *Advances in Neural Information Processing Systems*, 37:134841–134867, 2024.

A. Details of model architecture

A.1. Encoder

The role of the encoder is to embed the nodes and edges of the input graph into a high-dimensional space. For a routing problem instance \mathbf{s} , we represent it using a graph $G = (\mathcal{V}, \mathcal{E})$, where $\mathcal{V} = \{n_i \mid i = 1, 2, \dots, N\}$ and $\mathcal{E} = \{e_{i,j} \mid i, j = 1, 2, \dots, N\}$. The initial node features and edge features are respectively denoted as $\mathbf{n}_i^{\text{init}} \in \mathbb{R}^{F_n}$ and $\mathbf{e}_{i,j}^{\text{init}} \in \mathbb{R}^{F_e}$. The initial feature dimensions F_n and F_e depend on the problem settings.

As shown in Figure 1, the input features are first transformed into the embedding space \mathbb{R}^{d_m} with dimension $d_m = 128$ through an initial embedding layer:

$$\mathbf{n}_i^0 = \mathbf{W}_n^{\text{init}} \mathbf{n}_i^{\text{init}} + \mathbf{b}_n^{\text{init}}, \quad (20)$$

$$\mathbf{e}_{i,j}^0 = \mathbf{W}_e^{\text{init}} \mathbf{e}_{i,j}^{\text{init}} + \mathbf{b}_e^{\text{init}}, \quad (21)$$

where $\mathbf{W}_n^{\text{init}} \in \mathbb{R}^{d_m \times F_n}$, $\mathbf{W}_e^{\text{init}} \in \mathbb{R}^{d_m \times F_e}$, $\mathbf{b}_n^{\text{init}}, \mathbf{b}_e^{\text{init}} \in \mathbb{R}^{d_m}$.

After the initial embedding layer, the node and edge embeddings are updated through multiple encoder layers. The encoder layer consists of two main components: integrated attention layers and feed-forward layers. The integrated attention layer sequentially performs multi-head attention operations in the order of Node-Node, Edge-Node, and Node-Edge, enabling alternate updates of node and edge embeddings. The feed-forward layer comprises two linear layers with a ReLU activation function. Specifically, the embeddings are first transformed into a higher-dimensional space with dimension $d_{\text{ff}} = 512$ via the input linear layer, then passed through a ReLU activation, and finally projected back to dimension d_m by the output linear layer. Residual connections and normalization are applied to both the integrated attention layer and the feed-forward layer. Our model supports various normalization options, including batch, layer, and instance normalization. In the experiments presented in this paper, we employ instance normalization (Ulyanov et al., 2016). The computation of a single encoder layer proceeds as follows:

$$\hat{\mathbf{n}}_i^\ell = \text{MHA}(\mathbf{n}_i^{\ell-1}, [\mathbf{n}_1^{\ell-1}, \mathbf{n}_2^{\ell-1}, \dots, \mathbf{n}_N^{\ell-1}]) + \mathbf{n}_i^{\ell-1}, \quad (22)$$

$$\tilde{\mathbf{e}}_{i,j}^\ell = \text{MHA}(\mathbf{e}_{ij}^{\ell-1}, [\hat{\mathbf{n}}_i^\ell, \hat{\mathbf{n}}_j^\ell]) + \mathbf{e}_{ij}^{\ell-1}, \quad (23)$$

$$\tilde{\mathbf{n}}_i^\ell = \text{MHA}(\hat{\mathbf{n}}_i^\ell, [\tilde{\mathbf{e}}_{i,1}^\ell, \tilde{\mathbf{e}}_{i,2}^\ell, \dots, \tilde{\mathbf{e}}_{i,N}^\ell]) + \hat{\mathbf{n}}_i^\ell, \quad (24)$$

$$\mathbf{e}_{i,j}^\ell = \text{Norm}(\overline{\text{FF}}(\text{Norm}(\tilde{\mathbf{e}}_{i,j}^\ell))), \quad (25)$$

$$\mathbf{n}_i^\ell = \text{Norm}(\overline{\text{FF}}(\text{Norm}(\tilde{\mathbf{n}}_i^\ell))), \quad (26)$$

where $\overline{\text{FF}}$ denotes the feed-forward layer with residual connection. For input $\mathbf{x} \in \mathbb{R}^{d_m}$, $\overline{\text{FF}}$ is formulated as Equation (27). The parameter dimensions are $\mathbf{W}^{\text{ff},1} \in \mathbb{R}^{d_{\text{ff}} \times d_m}$, $\mathbf{W}^{\text{ff},2} \in \mathbb{R}^{d_m \times d_{\text{ff}}}$, $\mathbf{b}^{\text{ff},1} \in \mathbb{R}^{d_{\text{ff}}}$, $\mathbf{b}^{\text{ff},2} \in \mathbb{R}^{d_m}$.

$$\hat{\mathbf{x}} = \mathbf{W}^{\text{ff},2} \cdot \text{ReLU}(\mathbf{W}^{\text{ff},1} \mathbf{x} + \mathbf{b}^{\text{ff},1}) + \mathbf{b}^{\text{ff},2} + \mathbf{x}. \quad (27)$$

After processing through a total of L encoder layers, the final node embeddings $\{\mathbf{n}_i^L\}_{i=1,2,\dots,N}$ and edge embeddings $\{\mathbf{e}_{i,j}^L\}_{i,j=1,2,\dots,N}$ are obtained. For a given instance, the encoder is executed only once, extracting essential information from the input graph-structured data to assist the decoder in completing the designated task. The encoder structure is generally transferable and can be applied to other graph problems, such as the Maximal Independent Set problem.

A.2. Decoder

The proposed EGAM employs an autoregressive decoder structure that outputs the next node's probability distribution $p_{\theta}(\pi_t \mid \pi_{<t}, \mathbf{s})$ based on the historical path $\pi_{<t}$. We formulate this process as a Markov Decision Process, where the state at the current time step is represented by context information and the embeddings generated by the encoder. The embeddings $\{\mathbf{n}_i^L\}_{i=1,2,\dots,N}$ and $\{\mathbf{e}_{i,j}^L\}_{i,j=1,2,\dots,N}$ are static and contain information extracted from the problem instance. The context evolves dynamically throughout the decision-making process, with its design depending on the specific problem, as detailed in Section B. The initial context vector $\mathbf{n}_c^0 \in \mathbb{R}^{d_c}$ is embedded by a linear context embedding layer:

$$\mathbf{n}_c^0 = \mathbf{W}_c \hat{\mathbf{n}}_c + \mathbf{b}_c, \quad \mathbf{W}_c \in \mathbb{R}^{d_m \times d_c}, \quad \mathbf{b}_c \in \mathbb{R}^{d_m}. \quad (28)$$

Subsequently, similar to the encoder, we update \mathbf{n}_c^0 using attention layers and feed-forward layers. In the decoder layers, we employ node-node and node-edge attention mechanisms, treating \mathbf{n}_c^k (where $k = 0, 1, \dots, K$) as a node embedding. The

specific operations within a single decoder layer are as follows:

$$\hat{\mathbf{n}}_c^k = \text{MHA}(\mathbf{n}_c^{k-1}, [\mathbf{n}_1^L, \mathbf{n}_2^L, \dots, \mathbf{n}_N^L]; \mathbf{m}_c) + \mathbf{n}_c^{k-1}, \quad (29)$$

$$\tilde{\mathbf{n}}_c^k = \text{MHA}(\hat{\mathbf{n}}_c^k, [\mathbf{e}_{\pi_{t-1},1}^L, \mathbf{e}_{\pi_{t-1},2}^L, \dots, \mathbf{e}_{\pi_{t-1},N}^L]; \mathbf{m}_c) + \hat{\mathbf{n}}_c^k, \quad (30)$$

$$\mathbf{n}_c^k = \text{FF}(\tilde{\mathbf{n}}_c^k) + \tilde{\mathbf{n}}_c^k. \quad (31)$$

As shown in Equations (29) and (30), we incorporate a mask into the MHA operation to control the set of considered nodes. The mask $\mathbf{m}_c = [\mathbf{m}_{c,1}, \mathbf{m}_{c,2}, \dots, \mathbf{m}_{c,N}]$ is a Boolean vector where $\mathbf{m}_{c,i} = 1$ if node n_i is infeasible, and $\mathbf{m}_{c,i} = 0$ otherwise. This mask also constitutes part of the dynamic context information, evolving as the decoding process progresses. For example, in the TSP, nodes that have already been visited are excluded from consideration, and returning to the starting point is only allowed after all other nodes have been visited, thereby ensuring that the generated path satisfies the problem constraints.

The final probability is computed via a (masked) single-head attention layer. We perform a dot-product attention operation between the context embedding \mathbf{n}_c^K and adjacent edge embeddings $\{\mathbf{e}_{\pi_{t-1},j}^L\}_{j=1,2,\dots,N}$. The attention weights serve directly as the metric for node selection probabilities, thereby eliminating the need to compute the value vectors. The query and keys are projected using parameter matrices $\mathbf{W}_{\text{out}}^q, \mathbf{W}_{\text{out}}^k \in \mathbb{R}^{d_m \times d_m}$:

$$\mathbf{q}_c = \mathbf{W}_{\text{out}}^q \mathbf{n}_c^K, \quad \mathbf{k}_j = \mathbf{W}_{\text{out}}^k \mathbf{e}_{\pi_{t-1},j}^L \quad (32)$$

We then apply a clipped tanh function to limit the range of attention weights, followed by a softmax function to compute the final probabilities:

$$u_j = \begin{cases} \alpha \cdot \tanh\left(\frac{\mathbf{q}_c^T \mathbf{k}_j}{\sqrt{d_m}}\right), & \text{if } \mathbf{m}_{c,j} = 0 \\ -\infty, & \text{if } \mathbf{m}_{c,j} = 1 \end{cases} \quad (33)$$

$$p_{\theta}(\pi_t = n_i | \pi_{<t}, \mathbf{s}) = \text{softmax}_i(u_1, u_2, \dots, u_N). \quad (34)$$

Nodes are selected from $p_{\theta}(\pi_t | \pi_{<t}, \mathbf{s})$ using two decoding strategies: 1) greedy, i.e., $\pi_t = \text{argmax}_{n_i} (p_{\theta}(\pi_t = n_i | \pi_{<t}, \mathbf{s}))$; and 2) sampling according to the probability distribution. The decoder runs multiple times until the entire route is planned.

B. Adaptations to different routing problems

B.1. Travelling Salesman Problem (TSP)

Definition The TSP postulates a path planning scenario for a traveling salesman, aiming to identify the shortest possible route that visits each given location exactly once and returns to the origin. During instance generation, node positions are randomly distributed within a specified region, and the total tour length is computed using the Euclidean distance between nodes. The initial features include node coordinates and edge lengths.

Context The context for TSP contains the embeddings of the starting node and the previously visited node (the current node):

$$\hat{\mathbf{n}}_c = \text{Concat}(\mathbf{n}_{\pi_{t-1}}^L, \mathbf{n}_{\pi_1}^L). \quad (35)$$

Mask The mask for TSP in the decoder depends solely on the visited nodes. As indicated by Equation (36), nodes that have already been visited are masked, and returning to the starting node is permitted only after all other nodes have been visited.

$$\mathbf{m}_{c,i} = \begin{cases} 1, & \text{if } n_i \text{ has been visited} \\ 0, & \text{otherwise} \end{cases} \quad (n_i \neq \pi_1), \quad \mathbf{m}_{c,\pi_1} = \begin{cases} 0, & \text{All nodes have been visited} \\ 1, & \text{otherwise} \end{cases}. \quad (36)$$

B.2. Capacitated Vehicle Routing Problem (CVRP)

Definition The CVRP is defined as a path planning problem for vehicles with capacity constraints. It involves planning a set of routes, each starting and ending at a known depot, to serve a set of customer nodes. The core constraint is that the total demand of nodes served on a single route cannot exceed the vehicle's capacity. Consequently, a vehicle must return to the depot to be reloaded before this capacity limit is reached. The optimization objective is to minimize the total travel distance across all routes. Problem instances are constructed by randomly generating node locations and capacity demands. The initial features include node coordinates, demands (normalized) and edge lengths.

Context In CVRP, where the depot is fixed and specially embedded, the context incorporates the current node embedding and the remaining vehicle capacity:

$$\hat{\mathbf{n}}_c = \text{Concat}(\mathbf{n}_{\pi_{t-1}}^L, \text{Cap}(\boldsymbol{\pi}_{<t}, \mathbf{s})). \quad (37)$$

The remaining capacity is calculated as $\text{Cap}(\boldsymbol{\pi}_{<t}, \mathbf{s}) = C_0 - \sum_{\tau=1}^{t-1} D_{s, \pi_\tau}$, while C_0 denotes the total capacity and D_{s, π_τ} denotes the demand of node π_τ .

Mask Nodes are masked if they have already been visited or if their demand exceeds the remaining capacity of the vehicle. Additionally, the depot is always accessible.

$$\mathbf{m}_{c,i} = \begin{cases} 1, & \text{if } D_{s,i} > \text{Cap}(\boldsymbol{\pi}_{<t}, \mathbf{s}) \text{ or } n_i \text{ has been visited} \\ 0, & \text{otherwise} \end{cases}. \quad (38)$$

B.3. Prize Collecting Traveling Salesman Problem (PCTSP)

Definition The PCTSP extends the TSP by associating each node with a prize and a penalty. Specifically, a prize is collected if the node is visited, while a penalty is incurred if the node is skipped. A tour is deemed feasible only if the total prize collected from visited nodes meets or exceeds a predetermined threshold. The overall cost is defined as the sum of the tour length and the total penalties of nodes omitted from the tour. PCTSP also involves an additional depot serving as both the start and end point. The initial features include node coordinates, prize (normalized), penalty, and edge lengths.

Context The context for PCTSP includes the current node embedding and the remaining prize to be collected.

Mask The visited nodes are masked. The depot is masked until sufficient prize has been collected.

B.4. Travelling Salesman Problem with Time Window (TSPTW)

Definition The TSPTW imposes time window constraints on the nodes to be visited in the TSP. Each node must be visited before its deadline; otherwise, the visit is considered a failure. If arrival occurs earlier than the start of the time window, the agent must wait until the window opens. A tour is feasible only if all nodes are visited while satisfying these time constraints. To ensure the feasibility of instances, we adopt a generation function from the literature (Bi et al., 2024). For learning-based methods, a penalty term for time window violations is incorporated into the training cost, formulated as $C = L_{\text{tour}} + \beta \cdot (N_{\text{out}} + T_{\text{out}})$, where N_{out} and T_{out} denote the number of late-visited nodes and the total tardiness duration, respectively. We fix n_1 as the starting point and employ a separate initial embedding layer for it. The initial features include node coordinates, start time window, end time window, and edge lengths.

Context The context for TSPTW includes the current node embedding and current time.

Mask For TSPTW, we adopt a mask similar to that used in TSP. However, such a mask cannot guarantee solution feasibility, which is why we incorporate a penalty term into the cost function. In fact, ensuring the feasibility of solutions for TSPTW is a complex issue that has been studied in the work of (Bi et al., 2024), who proposed the PIP-mask. The PIP-mask can also be easily adapted for use in EGAM. Nevertheless, to compare the raw performance of the models, we did not employ it in the experiments presented in this paper.

B.5. Traveling Salesman Problem with Draft Limit (TSPDL)

Definition The TSPDL considers a ship routing problem for transporting goods between ports. Each node to be visited, representing a port, has a cargo capacity demand and a draft limit. The goal is to plan a route such that the ship's load at each port does not exceed the port's draft limit; otherwise, the route is considered infeasible. The locations, demands, and draft limits of the ports are generated according to specific distributions. The cost is defined as $C = L_{\text{tour}} + \beta \cdot (N_{\text{out}} + D_{\text{out}})$, where N_{out} and D_{out} represent the number of overloaded nodes and the total overload amount. The initial features include node coordinates, capacity demand, draft limit, and edge lengths.

Context The context for TSPDL includes the current node embedding and the current load.

Mask Similar to TSPTW, we use the same mask as TSP.

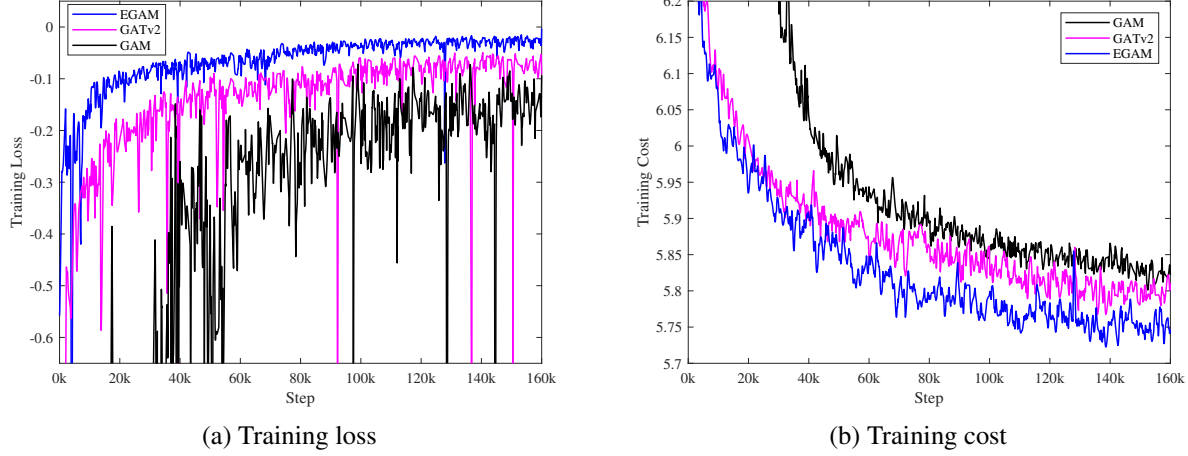


Figure 2. Evolution of the training loss and cost for TSP

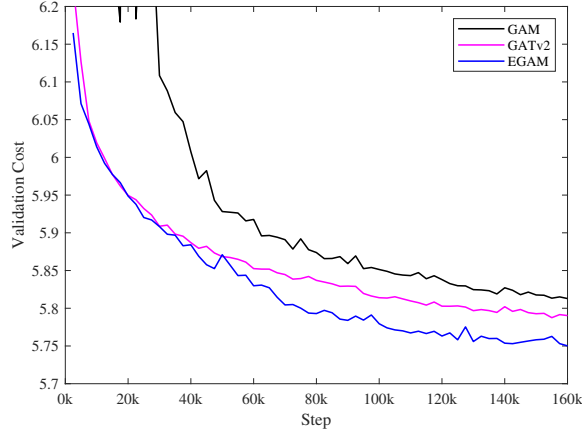


Figure 3. Evolution of the validation cost for TSP

B.6. Vehicle Routing Problem with Time Window (VRPTW)

Definition The classical VRPTW requires all nodes to be successfully visited. However, real-world routing problems often cannot guarantee conflict-free time windows. Hence, we relax this constraint by allowing routes to skip some nodes. In our formulation, the objective of VRPTW is to visit as many nodes as possible within their time windows, with the cost function being the number of unsuccessfully visited nodes. The initial features include node coordinates, start time window, end time window, and edge lengths.

Context The context for VRP includes the current node embedding and current time.

Mask For VRPTW, nodes whose time window ends before the current time are masked. Additionally, once the vehicle returns to the depot, the route is considered end.

C. Additional Experiments and Analysis

C.1. Training dynamics

To comprehensively investigate the training dynamics of different models, we monitor a suite of key performance metrics during the training process. Specifically, for TSP, we track the training loss, training cost, and validation cost to assess the optimization progress. For constrained routing problems such as TSPDL, we additionally monitor the feasible rate on both

training and validation sets to evaluate the model’s ability to satisfy problem constraints. All models are trained for 100 epochs, with each epoch comprising 2500 batches (treating one batch as one training step). The resulting learning curves, presented in the following figures, illustrate the evolution of these metrics for the proposed EGAM and baseline algorithms across different routing problems.

As illustrated in Figure 2 and Figure 3, EGAM demonstrates superior training characteristics on the TSP problem compared to GAM and GATv2. The training loss of EGAM exhibits a more rapid convergence toward zero, indicating more effective optimization of the learning objective. Concurrently, EGAM achieves a faster reduction in solution cost on both the training and validation sets, suggesting improved learning efficiency. These observations collectively demonstrate that EGAM offers advantages in terms of both convergence speed and solution quality.

For TSPDL, as shown in Figure 4 and Figure 5, EGAM simultaneously achieves superior performance in both solution quality and constraint satisfaction. During training, EGAM achieves a significantly higher feasible rate compared to GATv2 and Sym-NCO, while simultaneously attaining a lower solution cost. This indicates that EGAM not only learns to generate feasible solutions more reliably but also optimizes the solution quality within the feasible region. The consistent performance gap between EGAM and the baselines on both training and validation sets further validates the model’s robustness and generalization capability in handling constrained optimization problems.

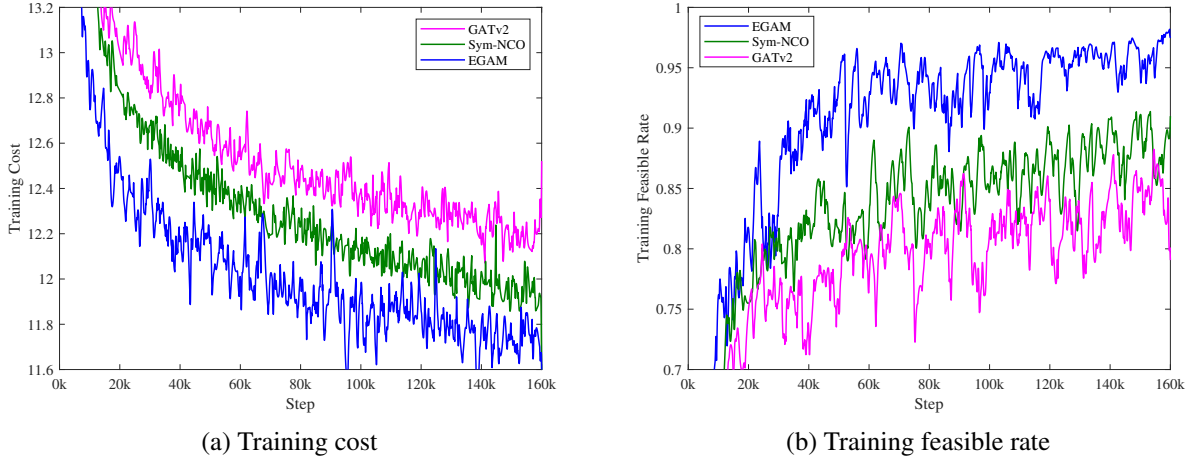


Figure 4. Evolution of the training cost and feasible rate for TSPDL

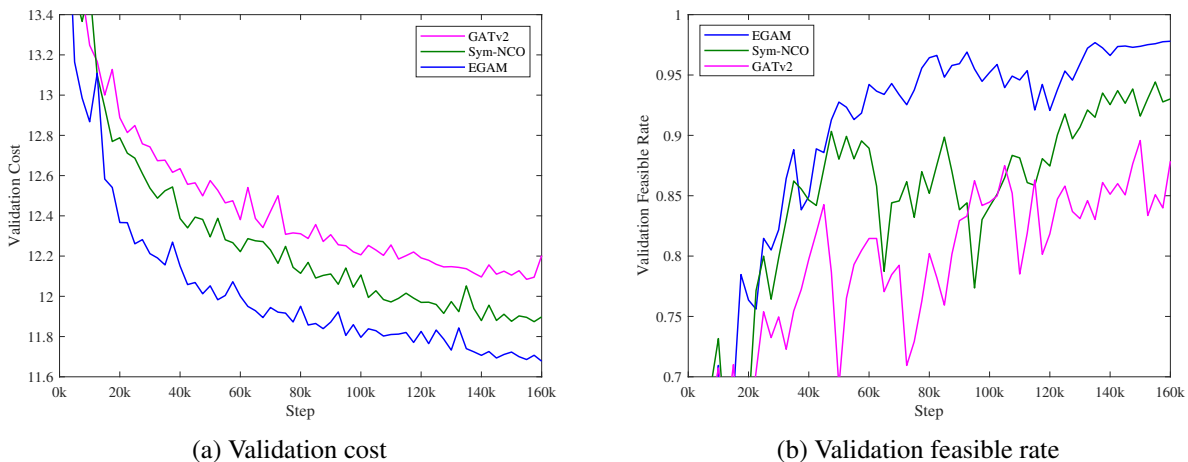


Figure 5. Evolution of the validation cost and feasible rate for TSPDL

C.2. Visualization of instances

To provide an intuitive illustration of routing problems and the solutions obtained by different NCO solvers, we visualize representative instances and their corresponding solutions in this section.

As shown in Figure 6, we present the solutions generated by different methods for a representative TSP instance. In this visualization, nodes to be visited are represented as dots, and the solution paths are depicted using arrows connecting the nodes. The starting point of each path is marked with a green dot to facilitate visual identification. The objective of TSP is to find the shortest possible route that visits all nodes exactly once and returns to the starting point, with no additional constraints imposed on the trajectory. Visual inspection reveals that all methods generate clear cyclic paths that form closed tours, which is consistent with the problem's structure. Notably, while the solution cost achieved by EGAM is very close to that of the optimal solution, subtle differences in the path structure can be observed. These differences, though minor in terms of cost, highlight the inherent complexity of routing problems where multiple near-optimal solutions may exist with distinct topological characteristics. Compared to traditional search-based solvers that require extensive computational time to find optimal solutions, EGAM demonstrates its capability to achieve near-optimal results efficiently, thereby showcasing its practical potential for real-world applications where computational resources are limited.

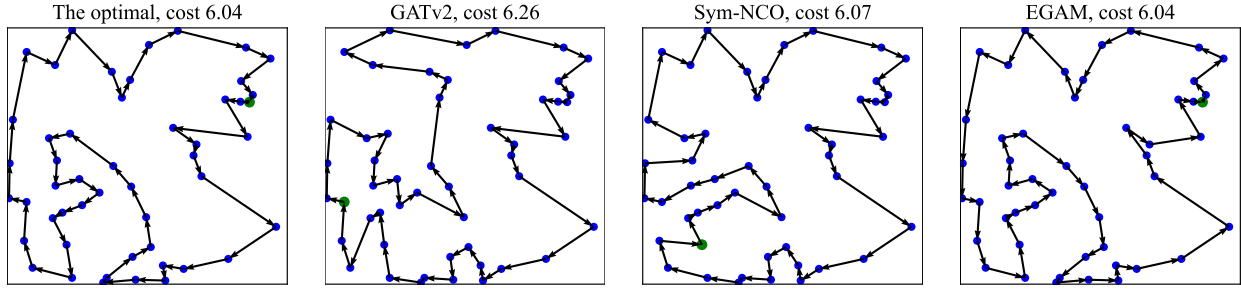


Figure 6. Visualization of TSP instance and solutions from different methods

The visualization of TSPTW results is presented in Figure 7. Compared to TSP, TSPTW introduces time window constraints for each node, requiring that the arrival time at each node falls within its specified time window. Only trajectories that satisfy the time windows of all nodes are considered feasible solutions. The data generation process ensures the existence of at least one feasible path for each instance. While the primary objective remains to minimize the total travel distance, the additional constraint significantly complicates the problem by restricting the feasible solution space. As illustrated in the figure, all methods, including EGAM and the baseline approaches (GATv2, Sym-NCO), successfully found feasible solutions that satisfy all time window constraints. However, EGAM achieved the shortest total travel distance among the feasible solutions, demonstrating its superior ability to optimize within the constrained solution space.

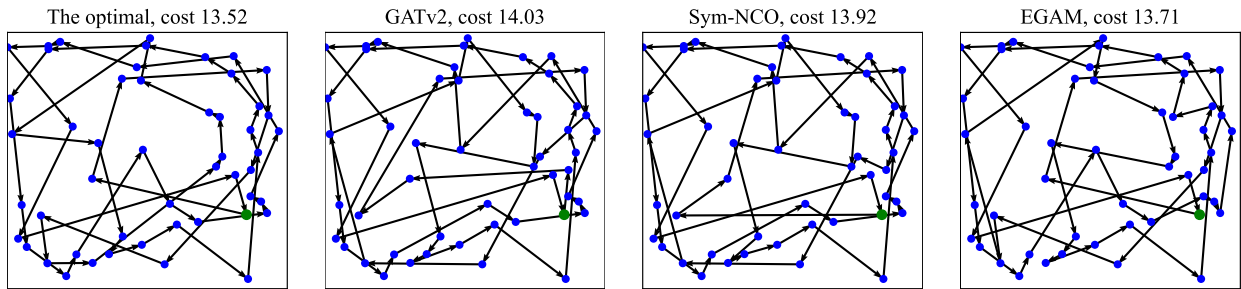


Figure 7. Visualization of TSPTW instance and solutions from different methods

For VRPTW, we consider a novel problem setting as described in Section B.6. In this modified VRPTW formulation, the objective shifts from minimizing travel distance to maximizing the number of nodes successfully visited within their respective time windows. This problem setting is particularly relevant for scenarios where service coverage is prioritized over travel efficiency. As shown in Figure 8, the visualization employs a color-coded scheme to distinguish different node states: blue points indicate successfully visited nodes that satisfy their time window constraints, red points represent nodes where visits were attempted but failed due to constraint violations, and gray points denote nodes that were not visited at all. The problem's cost is defined as the number of unsuccessfully visited nodes (i.e., the sum of failed and unvisited nodes),

making the objective equivalent to minimizing this cost or equivalently maximizing the number of successfully visited nodes. For the representative instance shown in the figure, EGAM successfully visited 34 nodes, outperforming Sym-NCO (33 nodes) and GATv2 (31 nodes).

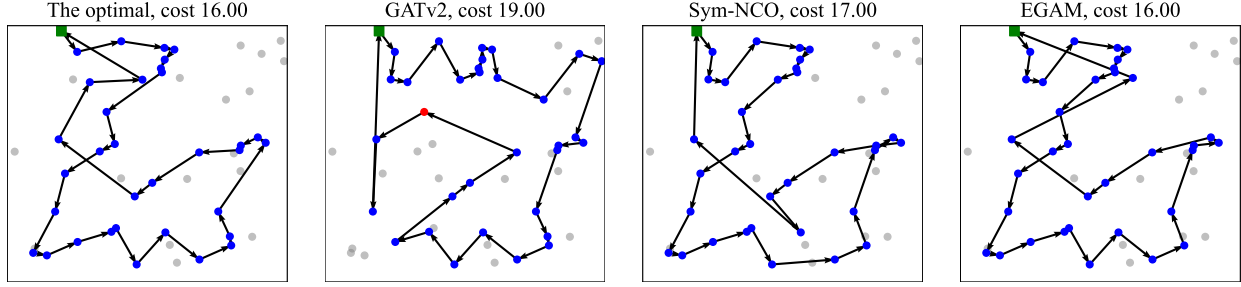


Figure 8. Visualization of VRPTW instance and solutions from different methods

C.3. Impact of the number of parameters

To assess the parameter efficiency of the proposed model, we conducted experiments to examine the impact of varying the number of encoder layers on model performance. We compare different layer configurations of EGAM and Sym-NCO on the VRPTW, analyzing both the number of parameters and the resulting performance, as summarized in Table 4.

Table 4. Impact of the number of parameters on Sym-NCO and EGAM

Method	Layers	Parameters	Performance on VRPTW
Sym-NCO	3	0.69×10^6	20.38
Sym-NCO	6	1.29×10^6	19.97
Sym-NCO	9	1.88×10^6	19.89
Sym-NCO	12	2.47×10^6	-
EGAM	3	1.70×10^6	19.82
EGAM	4	2.16×10^6	19.60

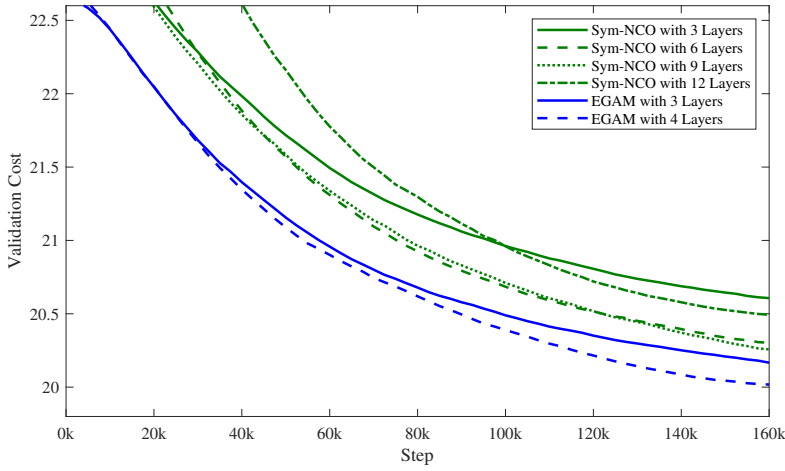


Figure 9. Validation cost curves during training for models with varying numbers of layers. For better clarity, an exponential smoothing with a coefficient of 0.9 was applied.

As shown in Table 4, EGAM requires more parameters per layer due to the simultaneous update of node and edge embeddings in each encoder layer. With a similar number of parameters, the 3-layer EGAM outperforms the 9-layer

Sym-NCO. Furthermore, when the number of parameters is large, the performance improvement from 9 layers to 6 layers in Sym-NCO is minimal. In contrast, the 4-layer EGAM shows a clear improvement over the 3-layer version. We attribute this to the network structure (as shown in Figure 1), where EGAM has a shallower depth for parameter gradient backpropagation, making it easier to train. We also present the validation cost curves during training for models with varying numbers of layers in Figure 9. From the figure, it is evident that the 12-layer Sym-NCO encounters significant training difficulties and struggles to converge (even after adjusting the learning rate, the issue persists). Additionally, the training cost for EGAM decreases more rapidly in the early stages compared to Sym-NCO. The two curves for EGAM consistently lie below the curves for Sym-NCO. These results indicate that our model architecture is more conducive to efficient parameter training, achieving faster convergence and better performance even with the same number of parameters.

C.4. Generalization performance

We evaluated the generalization capability of the proposed EGAM across different problem scales using generalization tests. Specifically, we considered three scales—20, 50, and 100—and assessed the models trained on corresponding datasets by testing them on datasets of other scales. Figure 10 presents a heatmap showing the performance gap of models trained on datasets of different scales but evaluated on the same problem scale. Table 5 provides the test results for models of the same problem scale. The average cost for each model, corresponding to the diagonal entries of Figure 10, is listed in the table.

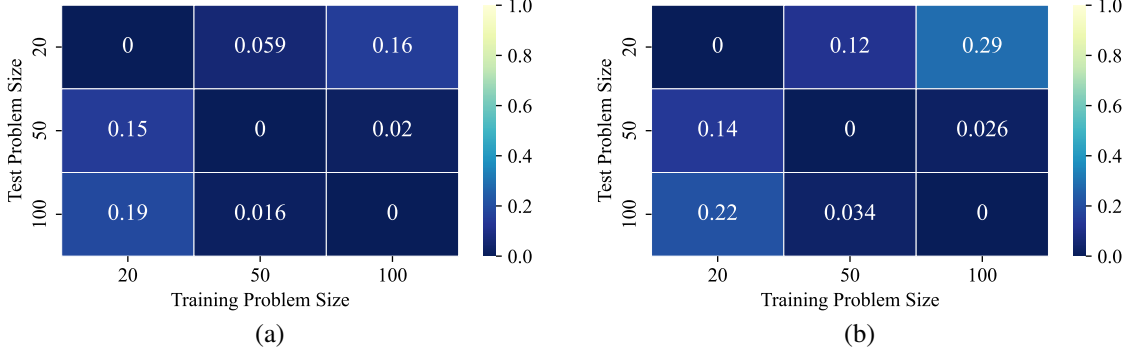


Figure 10. Generalization tests of EGAM (a) and Sym-NCO (b) trained and tested on VRPTW with various scales

Table 5. Performance of EGAM and Sym-NCO on VRPTW with different scales

Problem size	20	50	100
Sym-NCO	4.65	19.97	52.92
EGAM	4.58	19.60	52.53

As shown in Figure 10 (a) and (b), the diagonal elements are 0 because the models trained and tested on the same problem scale always perform the best. Comparing the two figures, it is evident that the performance gap between different EGAM models is smaller, indicating stronger generalization capability. The data in Table 5 further confirms that our model consistently outperforms the baseline across different problem scales.

D. Future Work

In this paper, we introduced the foundational model of EGAM within an autoregressive framework. Notably, EGAM demonstrates strong scalability. In future work, we aim to extend the application of EGAM to a broader range of scenarios, specifically in the following directions:

- Integrating improved methods tailored for NCO to enhance performance on specific problem types and larger-scale instances.
- Extending its application to a wider variety of routing problems, such as edge-based route planning.
- Exploring non-autoregressive architectures. By modifying the decoder, a non-autoregressive version of EGAM will output routing planning heatmaps, which can be trained using supervised learning.

- Generalizing the approach beyond routing problems to tackle a wider variety of combinatorial optimization tasks. Considering other combinatorial optimization problems, such as the Maximal Independent Set problem, many of which can also be represented as graph-based problems, we plan to leverage EGAM to efficiently address these challenges and establish a universal framework for graph-structured problems.

E. Licenses and Assets

In this work, we adopt existing routing solvers and neural combinatorial optimization methods as benchmarks for our experiments. The implementation of our innovations references the code frameworks developed by other researchers. The assets used in this work, along with their corresponding licenses, are listed in Table 6, all of which are available for academic use. Furthermore, we are also happy to release the source code developed in this study under the MIT License in the future, to facilitate communication and collaboration with other researchers.

Table 6. Assets used in this work

Asset	License	URL
Gurobi	Academic license for non-commercial use	https://www.gurobi.com/solutions/gurobi-optimizer/
OR-Tools	Apache-2.0 license	https://developers.google.com/optimization/routing/
LKH-3	Available for academic use	http://webhotel4.ruc.dk/~keld/research/LKH-3/
GAM	MIT license	https://github.com/wouterkool/attention-learn-to-route
POMO	MIT license	https://github.com/yd-kwon/POMO
PIP	MIT license	https://github.com/jieyibi/PIP-constraint